Highlights

Developing a risk-informed decision-support system for earthquake early warning at a critical seaport

Gemma Cremen, Francesca Bozzoni, Silvia Pistorio, Carmine Galasso

- The system integrates seismic risk predictions and multi-criteria decision-making
- The system identifies the optimal action (issue or not a warning) for a given event
- The optimal action can be sensitive to stakeholder risk preferences
- The optimal action can depend on the level of functionality interdependence captured

Developing a risk-informed decision-support system for earthquake early warning at a critical seaport

Gemma Cremen[a], Francesca Bozzoni[b], Silvia Pistorio[a,c], Carmine Galasso[a,c]

[a]*Department of Civil, Environmental and Geomatic Engineering, University College London, Chadwick Building, Gower Street, London, WC1E 6BT, United Kingdom*
[b]*European Centre for Training and Research in Earthquake Engineering (EUCENTRE), Via Adolfo Ferrata, 1, 27100, Pavia, Italy*
[c]*Scuola Universitaria Superiore (IUSS), Palazzo del Broletto, Piazza della Vittoria, 15, 27100, Pavia, Italy*

Abstract

Earthquake early warning (EEW) systems are used to provide timely alerts on ongoing earthquakes, which can facilitate important risk-mitigation actions before potentially damaging seismic waves reach target sites. A major shortcoming of existing EEW approaches is that the earthquake-related conditions for activating alerts are not generally defined according to a formal decision-support system (DSS) that accounts for possible risk-based consequences of triggering/not triggering the alarm. This paper exploits a next-generation risk-informed EEW DSS, which incorporates Multi-Criteria Decision-Making for evaluating the optimal decision. The proposed DSS integrates engineering-driven loss predictions associated with issuing/not issuing an EEW alert during an event, also considering possible system malfunctions. The DSS is demonstrated for the strategic Gioia Tauro seaport, located in the region of Italy with the highest seismic hazard. Real-time seismic risk analyses are conducted for various earthquake scenarios, accounting for event-parameter uncertainties that are integral to any EEW process and considering the multicomponent nature of the port as a system of interconnected elements. The results of these analyses are used as input to the proposed EEW DSS along with end-user risk preferences, to evaluate the optimal decision in each case and to define a series of risk-informed EEW warning thresholds for the port.

Keywords: earthquake early warning, decision-support system, port system, multi-criteria decision-making method, interdependencies

1. Introduction

The process of earthquake early warning (EEW) typically consists of the following steps: (1) detecting an earthquake during the early phases of fault rupture; (2) estimating the characteristics of the ongoing earthquake (e.g., in terms of its magnitude, location, and resulting ground shaking at target locations); and (3) issuing an alert to selected stakeholders that initiates risk-reduction actions before the arrival of potentially damaging seismic motions at their locations [e.g., 1]. The available lead (or warning) time between the alarm notification and the onset of strong shaking at a target site usually ranges from a few seconds to a few tens of seconds, which can facilitate automatic/rapid mitigation actions; examples include the slowing of high-speed trains, the activation of shut-off valves in gas pipelines, and the stepping away from hazardous locations in the workplace [2]. EEW systems operate in nine countries (including Japan and the USA), and are being tested for potential implementation in many more regions, including Southern Italy [3].

Many (if not all) existing operational EEW approaches (algorithms) employ relatively simplistic methods for determining when an alert should be issued [3]; decisions are typically based purely on a seismological threshold (such as magnitude or ground-motion amplitude) that are not adequately calibrated to capture/predict the impact of an incoming earthquake on the built environment [e.g., 4, 5, 6] and do not incorporate risk tolerance on the part of the end user(s). Maximising the utility of EEW requires the implementation of a formal decision support system (DSS) that explicitly accounts for the risk- and engineering-informed consequences of taking or not a particular risk-mitigation action, including the implications of unnecessarily raising an alarm, and stakeholder preferences/priorities towards different types of risks [7]. This paper explores the development of such a risk- and engineering-oriented EEW DSS for specific application to seaport systems, which act as crucial nodes that facilitate the critical process of maritime transportation [8, 9]. In doing so, it represents the first attempt to consider and demonstrate EEW in the context of a port. This type of EEW approach must account for a complex seismic response across a system of interconnected components upon which the successful daily operation of a port is dependent (and where reliability literature has thus far focused) [e.g., 10, 11, 12, 13, 14].

The examined case study is the port of Gioia Tauro, which is the largest

terminal for transshipment in Italy and one of the most important hubs for container traffic in the Mediterranean Sea. It is located within the Calabria region in Italy characterized by high seismicity [15] and it represents a priority entry point that could play a crucial role in post-earthquake disaster relief efforts [16, 17]. For these reasons, the port of Gioia Tauro was selected as one of the testbeds within the 2019-2022 European H2020 project named TURNkey (*Towards more earthquake-resilient URban societies through a multi-sensor-based informatioN system enabling earthquaKe Forecasting, early warning and rapid response actions*); the multi-sensor TURNkey unit (including low-cost accelerometers) has been deployed within the port area to facilitate EEW for this critical infrastructure.

The end-to-end EEW DSS for the port of Gioia Tauro is developed by leveraging and implementing existing tools, i.e. decision-making algorithms and a seismic risk assessment methodology for port systems, within a novel harmonized framework. The DSS specifically combine/unifies: (1) the framework of Performance-Based Earthquake Early Warning, or PBEEW [18, 19, 20], which uses a probabilistic, engineering-based risk model to determine whether EEW alerts are triggered; (2) a simulation-based risk assessment methodology, proposed by Conca et al. [21], that generates damage and loss scenarios accounting for the systemic vulnerability of the multi-component port system and its interdependent functionality; and (3) a multi-criteria decision-making (MCDM) algorithm [22], that builds on the engineering-oriented consequence predictions and was previously applied to a EEW DSS by Cremen and Galasso [7]. The purpose of the MCDM component is to account for the risk preferences/priorities of stakeholders across various dimensions of risk that do not necessarily need to be measured in a consistent unit.

The developed DSS specifically considers two possible actions, i.e., "trigger" or "don't trigger" an EEW alarm for an incoming earthquake, which are evaluated according to different stakeholder-weighted loss/consequence metrics that respectively account for their implications in terms of public safety (potential for casualties) and economic considerations (potential for delays to port operations). Ground-motion estimates (or proxy indicators based on early event data) from an EEW algorithm are input to the simulation-based risk assessment framework, which is used to determine action-specific loss predictions according to the PBEEW framework. These predictions are finally coupled with the decision-making algorithm, to identify the optimal action for the particular scenario of interest.

The paper is organised as follows. Section 2 presents the case study, describing the main elements of the port and illustrating their interdependencies, starting from a brief illustration of the interdependency model that was previously presented in the literature by Conca et al [21]. We then propose an upgraded version of the Conca et al. [21] model that accounts for additional port-component interdependencies. Section 3 describes the development and application of the EEW DSS to the port system, including sensitivity analyses for the application on some main sources of variability (i.e. the interdependency models and decision-making inputs). The main findings and potential further developments of this work are finally discussed in the concluding section.

2. Case Study Description

The seaport of Gioia Tauro plays a strategic role in the maritime transport network of Italy, as the largest terminal for container throughput in the country. More than one-third of all national transshipment traffic in Italy takes place at the port of Gioia Tauro, based on maritime traffic data available across different years on international platforms (e.g. `https://www.contshipitalia.com/en/connectivity`; `https://www.evergreen-marine.com/`; `https://web.archive.org/web/20210415031820/`; `https://www.msc.com/`). It is also one of the most important transshipment hubs in the Mediterranean Sea, connecting the global and regional networks that cross one of the busiest seas in the world. Furthermore, the port is located within the Calabria region in Southern Italy, which is characterized by the highest seismic hazard in the country. Figure 1 displays the seismogenic sources around the port. In this context, the port of Gioia Tauro plays a key role for Civil Protection rescue operations [16] by serving as a priority entry point into a territory potentially affected by strong earthquakes with moderate-to-large magnitudes.

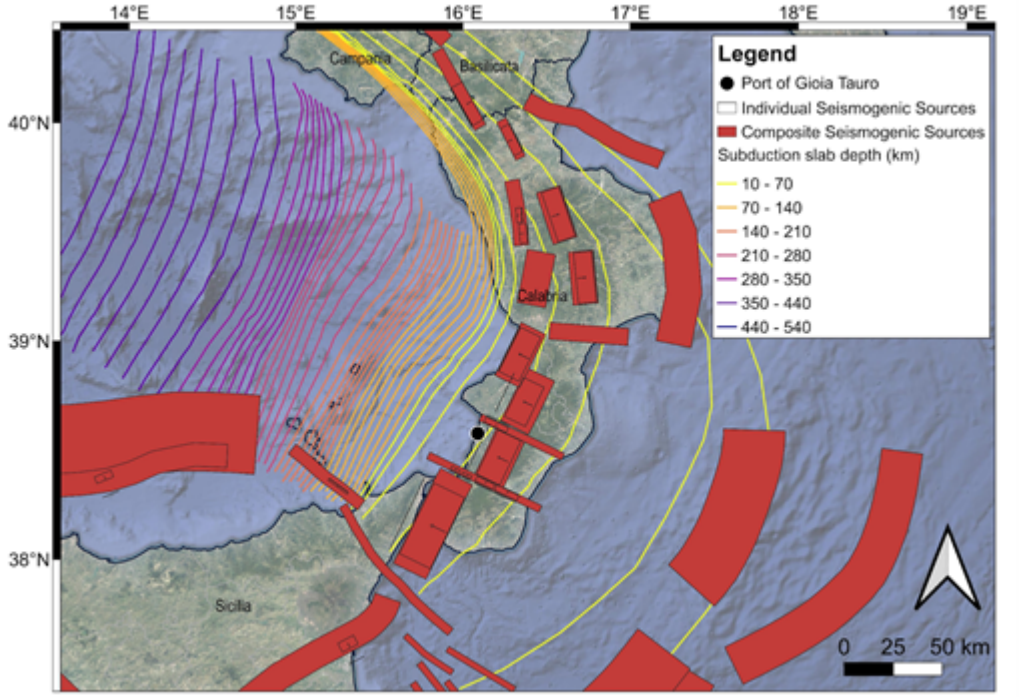

Figure 1: Map of the seismogenic areas according to the Database of Individual Seismogenic Sources [23] around the case-study port of Gioia Tauro (black dot in the map), located in Southern Italy, within the Calabria Region.

The port consists of an artificial channel, 200m (min) - 250m (max) wide and 3km long, running parallel to the coastline with a 300m wide entrance and an evolution basin of 750m in diameter [24]. It has eight docks with extensions of 5,125m and is composed of interconnected structural and infrastructural elements that constitute a framework supporting the functionality of the entire multicomponent system. Indeed, a variety of facilities exists within the seaport of Gioia Tauro, such as different typologies of wharf structures, infrastructure for cargo handling and storage, utility systems (e.g. electric power system), etc. A GIS (Geographical Information System) database of the multicomponent seaport system was built by Bozzoni et al. [24] and recently updated using data provided by the Port Authority.

This study exclusively considers the highlighted terminals in Figure 2 used for container operations, in line with Conca et al. (2020). Each port terminal represents a subsystem of the port and is composed of waterfront structures (wharves), operating cranes, and the electric power system, which

is represented in this study as an electric cabin (i.e., substation). The port's activities (around ship traffic and terminal handling operations) are supervised and coordinated from one central control office, which is also included in our analyses, along with seven other buildings that house the Port Authority, first responders operating within the port area, such as the firefighter local unit, etc.

Figure 2: Map of the case-study Gioia Tauro port, which is a complex system of various components including wharves, cranes, an electric power system, strategic buildings, etc. The three main terminals considered in this study, namely Alti Fondali, Levante ABC and Levante D, are highlighted in the map.

The functionality interdependency model proposed by Conca et al. [21] for the port - hereinafter referred to as the *"original interdependency model"* - is adopted as a starting point in this study. This model incorporates various levels of interdependencies across the port's multiple components, and

we exclusively account for those related to container handling operations in this study. The first considered interdependency involves the cargo handling equipment and the electric power system. A crane is deemed to be out of service if it is not provided with power by the corresponding electric cabin and it does not have a back-up power supply. The second type of interdependency leveraged in this study involves the cranes and the corresponding waterfront structure on which each crane is located; a crane may be rendered out of service due to the damage experienced by the wharf along which it usually operates during cargo handling. We integrate a further level of interconnected functionality in this study, presented in Figure 3. The control office is a strategic component of the port, since it is used to oversee all of its operations. If this office is structurally damaged or not receiving power from the corresponding electric cabin, it is herein assumed that the container handling operations of the terminals cannot function. We also incorporate a more realistic characterisation of electricity supply to the terminals than that of the original interdependency model (according to recently gathered information on the port), such that the total power across all examined terminals is assumed to be provided by one electric cabin (rather than three). The complete set of port functionality interdependencies considered in this work is hereinafter referred to as the *"proposed interdependency model"*.

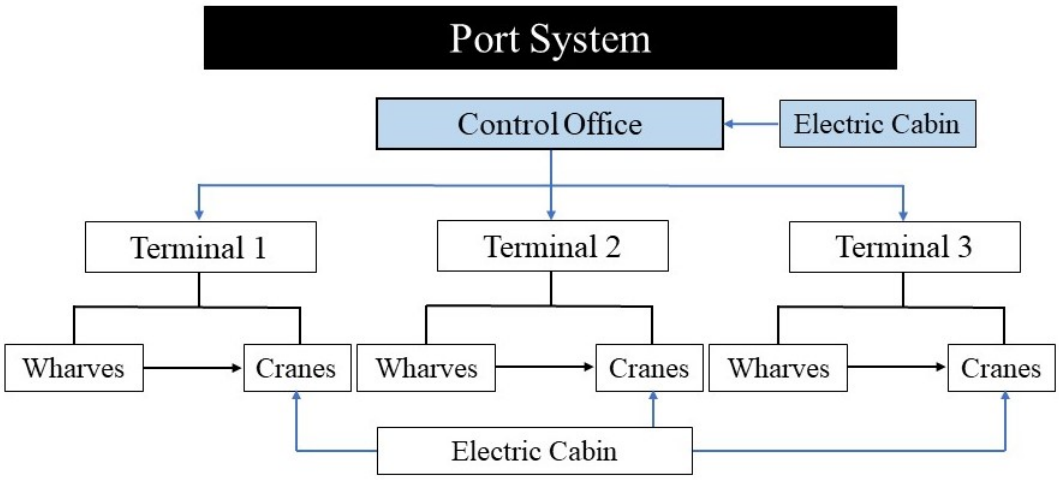

Figure 3: Representation of the functional interdependencies among port elements considered in this study. White boxes and black arrows indicate interdependencies of the original interdependency model, described in Conca et al. [21]. Light blue boxes and arrows indicate additional interdependencies introduced in this study.

3. Development and Application of the Proposed Risk-informed EEW DSS

This section describes the conception of a risk-informed EEW DSS for application to a port system, with specific reference to the Gioia Tauro case study presented in Section 2. Note that in the absence of validated EEW- and risk-related models that have been specifically designed for the port of interest, a number of potentially simplified assumptions (details to follow) are made in the course of this application. This implies that the results of the case study should be treated as a hypothetical demonstration of the methodology, with further site-specific data collection/verification required to determine their validity in a real-life practical implementation of the proposed EEW DSS. The general workflow for developing the DSS is shown in Figure 4 and is briefly described as follows:

- *Step 1: Identification of EEW actions for mitigating earthquake impacts.* Risk-mitigating actions that can be taken when an EEW alert is issued are defined according to the specific context under investigation (e.g., the potential strength of incoming shaking, the available lead-time, stakeholder perspectives, etc.) and the end-user-specified target structures/infrastructure to be protected. Possible actions include activating sirens to evacuate buildings and shutting down electrical systems to avoid damage (from fires or otherwise)/minimize post-event disruption.

- *Step 2: Quantification of event estimates, using an EEW algorithm.* EEW algorithms typically translate input parameters related to early seismic signals of ongoing earthquakes into estimates of relevant event characteristics (magnitude and location) and/or related ground-motion Intensity Measures (IMs). Event estimates are characterised by some bias and uncertainty, given the empirical/analytical nature of the algorithms and the fact that the EEW parameters evolve in time [25].

- *Step 3: Risk assessment of the port system.* This assessment connects the previous two steps, by evaluating the consequences of the identified EEW mitigation actions (plus the case of taking no action) according to the estimated earthquake characteristics provided by the EEW algorithm, also accounting for potential system malfunctions (i.e., false/missed alerts).

- *Step 4: Application of the decision-making algorithm.* The decision-making algorithm translates the consequences computed in the previous step into appropriate decision metrics, from which the optimal decision (i.e., issue or do not issue an alarm) is computed.

- *Step 5: Definition of optimal decision thresholds.* The previous three steps are repeated across a range of earthquake scenarios, to calibrate optimal decision thresholds, i.e., the conditions under which the optimal decision switches from not issuing to issuing the alarm. These thresholds can be expressed in terms of different seismological metrics that are output/used by the EEW system, including IMs, magnitude-distance pairs, or the raw parameters that act as inputs to conventional EEW algorithms. The thresholds can be computed offline and stored in a database/lookup table, for efficient real-time decision making during an earthquake.

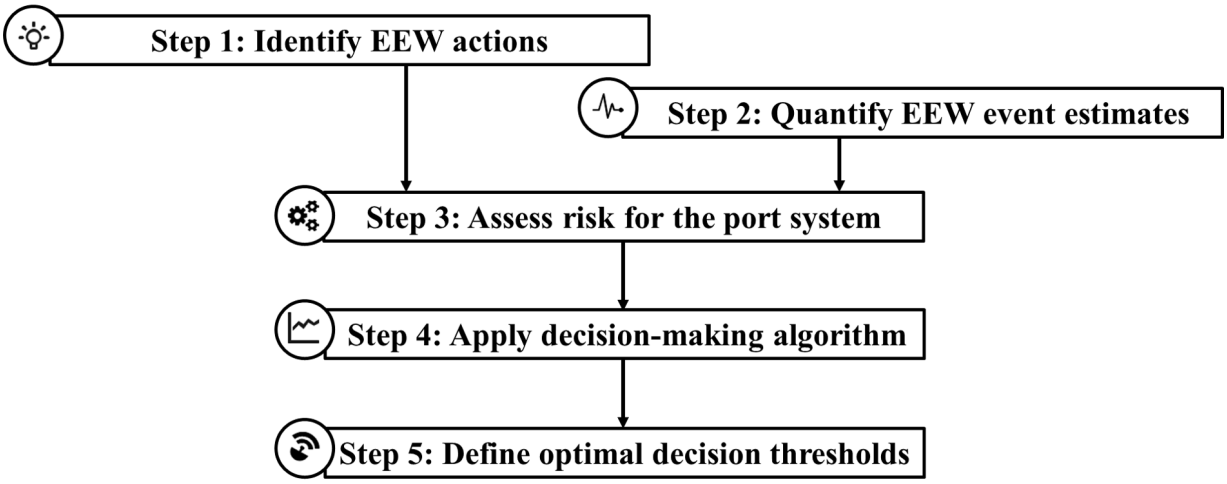

Figure 4: Workflow proposed in this study for developing a risk-oriented DSS for an EEW system at a port.

3.1. Step 1: Identification of EEW actions for mitigating earthquake impacts

EEW actions for the port of Gioia Tauro were identified in consultation with the port's infrastructure manager, who is a potential end user of the EEW system. The first action identified (Action #1) was the automatic issuance of siren warnings (potentially including pre-recorded messages) that

alert port workers to take rapid safety measures, such as Drop, Cover and Hold On [26]. The second identified action (Action #2) was the automatic shut-down of the port's electric power system, which could potentially eliminate the threat of earthquake-induced fires that may cause large disruptions to port operations, given the complex interconnected nature of its components. It is assumed that both actions would be carried out if an alert was issued. Note that since an EEW system does not yet operate at the port, the aforementioned actions were determined without consideration of potential lead times. However, typical times required to perform Action #1 and Action #2 are less than 10 seconds [e.g., 27, 28], which is in line with the potential amount of EEW lead time available in Italy [29]

3.2. Step 2: Quantification of event estimates, using an EEW algorithm

We consider a series of different algorithms in this study. The first two are idealised models (Algorithm #1 and Algorithm #2), which are respectively able to estimate the associated ground-shaking IMs in terms of ground-motion amplitude (im), and the magnitude-location (i.e., source-to-site distance) parameters ($M^* - R^*$) of the incoming earthquake, with no bias or uncertainty. Let $\mathbf{d}$ denote current (early) knowledge on an incoming event provided by measurements on a series of seismic instruments. Thus, $\mathbf{d} = im$ for Algorithm #1 and $\mathbf{d}$ is equivalent to the ($M^* - R^*$) couple for Algorithm #2.

The final considered algorithm (Algorithm #3) more realistically reflects the capabilities of current operational EEW systems, which generally predict event parameters based on early physical measurements recorded at near-fault seismic stations. Algorithm #3 specifically involves the following Bayesian formulation developed in Iervolino et al. [25], which estimates the magnitude of the incoming event based on the predominant period measured in the first four seconds of a P-wave recording (τ_i):

$$f(m|\mathbf{d}) = f(m|\hat{\tau}) = \frac{e^{2\mu_{\ln(\tau)} \sum_{i=1}^{n} \ln(\tau_i) - n\mu^2_{\ln(\tau)}/2\sigma^2_{\ln(\tau)}} e^{-\beta m}}{\int_{M_{min}}^{M_{max}} e^{2\mu_{\ln(\tau)} \sum_{i=1}^{n} \ln(\tau_i) - n\mu^2_{\ln(\tau)}/2\sigma^2_{\ln(\tau)}} e^{-\beta m}\, dm} \quad (1)$$

where $f(m|\hat{\tau})$ represents the probability density function (pdf) of the incoming earthquake's magnitude, conditional on the geometric mean of the algorithm's input parameters measured across n stations ($\hat{\tau}$). The lognormal parameters for $\hat{\tau}$ are obtained from the magnitude-scaling relationships derived by Allen and Kanamori [30], i.e.,

$$\mu_{\ln(\tau)} = \frac{m - 5.9}{7\log_{10}(e)} \tag{2}$$

and

$$\sigma_{\ln(\tau)} = \frac{0.16}{\log_{10}(e)} \tag{3}$$

$\beta = \ln(10)b$, b is the slope of the Gutenberg-Richter relation, and M_{max} and M_{min} are respectively the maximum and minimum considered magnitudes. Herein, we take $\beta = 1.56$, $M_{max} = 7.6$, and $M_{min} = 4.3$, which are the parameter values associated with the relevant zone 929 of the Italian seismic source model [15, 31]; M_{min} and M_{max} are assumed to correspond to moment magnitude values in this case, in line with Picozzi et al. [32]. We assume that Algorithm #3 can estimate location accurately and with certainty (i.e., that the information provided by n seismic stations can be used to directly compute the correct site-to-source distance R^*), which is a reasonable supposition even for practical EEW approaches to event estimation [25].

3.3. Step 3: Risk assessment for the port system

This assessment separately considers the consequences to the port facility associated with taking no action and issuing an alarm.

3.3.1. Risk assessment for the "no alert" case

If no EEW alarm is issued, the consequences of the impending ground shaking can be predicted using a well-established seismic risk assessment methodology. We leverage the simulation-based risk methodology developed by Conca et al. [21] for the port of Gioia Tauro, which incorporates the functional interconnections of the *original interdependency model* described in Section 2. This approach uses Monte Carlo sampling to approximate the following triple integral for a given scenario earthquake:

$$E(L|M^*, R^*) = \int_L \int_{DS} \int_{IM} l\, f(l|ds)\, f(ds|im)\, f(im|M^*, R^*)\, dL\, dDS\, dIM \tag{4}$$

where $E(L|M^*, R^*)$ denotes the expected loss for the considered event of magnitude M^*,with site-to-source distance R^*. IMs are first sampled according to the $f(im|M^*, R^*)$ pdf, which can be obtained from a Ground-Motion Model (GMM), for example. The simulated IMs are then used to estimate the extent of damage (ds) to vulnerable port components, based on appropriate

fragility relationships represented by the $f(ds|im)$ pdf. Note that fragility relationships for the *original interdependency model* are largely obtained from HAZUS [33], in line with Conca et al. [21]; the fragility model for wharves is instead selected according to Bozzoni and Lai [34]. Information on damage is translated to port losses (l) using damage-to-loss relationships described by the $f(l|ds)$ pdf, accounting as necessary for the functional interdependencies of the *original interdependency model*. We adapt equation 4 for EEW purposes, by integrating the PBEEW framework proposed by Iervolino et al. [19] as follows:

$$E(L_{NA}|\mathbf{d}) = \int_L \int_{DS} \int_{IM} l\, f'(l|ds)\, f'(ds|im)\, f(im|\mathbf{d})\, dL\, dDS\, dIM \qquad (5)$$

where the NA subscript denotes the "no alert case". Both $f'(ds|im)$ and $f'(l|ds)$ account for the *proposed interdependency model*, as well as the seven additional port buildings considered in this study (see Section 2); note that building fragility functions are those presented in Borzi et al. [35, 36] for generic 4-story reinforced concrete structures with earthquake-resistant design that are calibrated based on Italian data. The conditioning vector $\mathbf{d}$ is as defined in Section 3.2. For Algorithm #1, $\mathbf{d}$ is equivalent to the peak ground acceleration (PGA) associated with the incoming event (given the formulation of the adopted fragility relationships, although other IMs better correlated with engineering damage could be used if available) and Equation 5 reduces to:

$$E(L_{NA}|pga) = \int_L \int_{DS} l\, f'(l|ds)\, f'(ds|pga)\, dL\, dDS \qquad (6)$$

For Algorithm #2 (where $\mathbf{d}$ is equivalent to the $(M^* - R^*)$ couple; see Section 3.2), $f(im|\mathbf{d}) = f(pga|\mathbf{d})$ is derived from a two-step process. Firstly, PGA values for rock conditions are simulated according to the hypocentral-distance version of the Akkar et al. [37] GMM for Europe, which is applicable across the $[M_{min}, M_{max}]$ range of magnitudes relevant for the case study. Note that unknown faulting conditions are assumed, to reflect typical limitations of EEW algorithms [38], such that the style-of-faulting dummy variables in the GMM are set to zero. The sampled rock ground-motion intensities are then modified to account for the local site effects described in Bozzoni et al. [24], using the simplified approach based on litho-sratigraphic amplification factors from the Italian Building Code [39]. In the case of Algorithm #3,

$\mathbf{d} = \hat{\tau}$ and $f(im|\mathbf{d}) = f(pga|\mathbf{d})$ can be obtained according to:

$$f(pga|\mathbf{d}) = f(pga|\hat{\tau}) = \int_M f(pga|m, R^*)\, f(m|\hat{\tau})\, dM \tag{7}$$

where $f(m|\hat{\tau})$ is computed using equation 1, $f(pga|m, R^*)$ is obtained in the same way as $f(pga|\mathbf{d})$ for Algorithm #2, and all other variables are as previously defined.

We consider two types of loss (L) in this study, i.e., port performance loss (which measures the total reduction in containers that the port can handle), and the number of casualties among port workers.

Port performance loss. Port performance loss (PI_{loss}) is a risk metric proposed in this study, combining the earthquake-induced daily reduction in containers that the port can handle $PI_{loss/day}$ and downtime DT, which represents the time to repair and restore damaged components of the *proposed interdependency model*. It is computed for the "no alert" case according to the following equation:

$$E(PI_{loss,NA}|\mathbf{d}) = E(PI_{loss/day,NA} \times DT_{NA}|\mathbf{d}) \tag{8}$$

$PI_{loss/day,NA}$ is calculated as the loss of crane capacity in twenty-foot equivalent units per day (TEU; in line with Conca et al. [21]). The jth Monte Carlo iteration $PI^j_{loss/day,NA}$ is obtained according to the following set of rules that form the basis of the *proposed interdependency model* and are consistent with the *ds*-dependent functionality assumptions of the *original interdependency model*:

1. An electric cabin is operational if its sampled *ds* is lower than moderate (i.e., there is a failure in less than 5% of circuit breakers or disconnect switches) .
2. A crane is functional if it is receiving an electrical supply, its *ds* and that of the corresponding wharf are both lower than moderate (i.e., major repairs are not required), and the control office is operational.
3. The control office is operational if its sampled structural *ds* is less than moderate (i.e., there is no structural damage) and if it is receiving an electrical supply.

DT_{NA} separately consists of the time required to restore the structural elements of each terminal, the port's electricity supply, and the control office.

In line with the $PI_{loss/day,NA}$ metric, all components with sampled ds less than moderate are deemed functional (and are consequently assigned 0 days of downtime). Downtimes used for all other ds are obtained from information provided in the HAZUS methodology [40]. ds-dependent downtimes for the control office are set equal to the "GOV2" (emergency response) occupancy class building recovery times provided in Table 11-8 of HAZUS [40]. For all other components, downtimes are assigned as the duration until the first day on which the probability of functionality is 100% according to the corresponding restoration curve (Table 7-16 of HAZUS [40] is used to determine crane and wharf restoration curves, and the first row in Table 8-27 of HAZUS [40] is used to develop the electric cabin's restoration curve). We assume that all elements of the same type are repaired in parallel, such that the jth Monte Carlo simulation of downtime for the kth element type of the ith terminal is computed as follows:

$$DT^{j}_{element,NA,k,i} = \max\{DT^{j}_{element,NA,k,i,1}, DT^{j}_{element,NA,k,i,2}, \ldots, DT^{j}_{element,NA,k,i,n_k}\} \tag{9}$$

where n_k is the total number of element type k in the ith terminal. Then, the total downtime of the ith terminal assumes that its n_e different element types are repaired in series, as follows:

$$DT^{j}_{terminal,NA,i} = \sum_{k=1}^{n_e} DT^{j}_{element,NA,k,i} \tag{10}$$

We assume that each of the considered n_t terminals are repaired sequentially, such that the total downtime attributable to terminals ($DT^{j}_{total\,terminal_{NA}}$) is:

$$DT^{j}_{total\,terminal_{NA}} = \sum_{i=1}^{n_t} DT^{j}_{terminal,NA,i} \tag{11}$$

Finally, the total downtime of the port is computed according to:

$$DT^{j}_{NA} = DT^{j}_{total\,terminal_{NA}} + DT^{j}_{total\,electric_{NA}} + DT^{j}_{total\,building_{NA}} \tag{12}$$

where $DT^{j}_{total\,electric_{NA}}$ is the downtime of the electric cabin and $DT^{j}_{total\,building_{NA}}$ is the recovery time of the control office.

Port worker casualties. The HAZUS casualty module is used for quantifying the number of port worker casualties (NC).We estimate the total number of

workers at the port of Gioia Tauro as 1200, based on a previous European Commission Report [41]. We assume that this number excludes crane operators, is equally distributed among the port's eight considered buildings, and consists of 700 indoor and 500 outdoor day (08:00-19:00) workers, where the latter values are respectively decreased by 60% and 40% for night-time hours. Indoor ($CR^j_{indoor,NA,n,s}$) and outdoor ($CR^j_{outdoor,NA,n,s}$) casualty rates of the sth severity level at the nth building in the jth Monte Carlo simulation are respectively obtained from Tables 12-3 to 12-7 and 12-9 to 12-11 of HAZUS [40] based on the simulated ds, and assuming a 100% probability of collapse for the complete damage state to comply with the functional form of the building fragility functions [35, 36]. Then, the number of port-worker casualties for the kth building in the jth Monte Carlo simulation is calculated from:

$$NC^j_{NA,k} = N^j_{indoor,NA} \sum_{s=1}^{4} CR^j_{indoor,NA,n,s} + N^j_{outdoor,NA} \sum_{s=1}^{4} CR^j_{outdoor,NA,n,s} \tag{13}$$

where $N^j_{indoor,NA}$ and $N^j_{outdoor,NA}$ respectively denote the building's indoor and outdoor occupancy number, which is determined from a uniform sampling of time for each simulation. The number of crane-worker casualties for the jth simulation ($NC^j_{cranes,NA}$) is computed as the total number of cranes for which the sampled ds is extensive. The expected number of total port-worker casualties in the case of no alarm is finally computed as:

$$E(NC_{NA}|\mathbf{d}) = \sum_{k=1}^{n_b} E(NC_{NA,k}|\mathbf{d}) + E(NC_{cranes,NA}|\mathbf{d}) \tag{14}$$

where n_b is the total number of considered buildings (i.e., 8). $E(NC_{NA,k}|\mathbf{d})$ and $E(NC_{cranes,NA}|\mathbf{d})$ are respectively the average values of $NC^j_{NA,k}$ and $NC^j_{cranes,NA}$ across all Monte Carlo simulations.

3.3.2. Risk assessment for the "alert" case

Expected losses that occur in the case of issuing the alarm $E(L_A|\mathbf{d})$ are considered to be a combination of: (1) a mitigated quantity of the losses that would occur for the given earthquake scenario if no alert was issued; (2) the cost of implementing the associated preventative actions; and (3) the losses associated with unnecessarily taking action due to a potential system malfunction. Both (1) and (2) relate to losses that occur in the case of

a "true alarm", whereas (3) represents the "false alarm" case. Action #1 (i.e., activating warning sirens; see Section 3.1) is assumed to eliminate all building-related non-collapse casualties that would occur in the case of no alarm, but cause a 1% probability of one casualty in each non-collapsed building (due to panic) for either a true or a false alarm. Action #2 (shutting down the electricity supply; see Section 3.1) is assumed to reduce the damage that would occur to the electric cabins for the no alarm case by one level, but to cause downtimes of one day for inspection checks (if an alarm is falsely issued) and restoring electric power (in the case of either a true or a false alarm). The combined effect of Actions #1 and #2 are expressed in the following equations:

$$E(NC_A|\mathbf{d}) = 0.01 \times \sum_{k=1}^{8}(1 - p(\text{Collapse}_k|\mathbf{d}) + \sum_{k=1}^{8} p(\text{Collapse}_k|\mathbf{d}) \times E(NC_{NA,\text{collapse},k}|\mathbf{d}) + E(NC_{cranes,NA}|\mathbf{d}) \tag{15}$$

$$E(PI_{loss,A}|\mathbf{d}) = E(PI'_{loss,NA}|\mathbf{d}) + E(PI'_{red/day}|\mathbf{d}) \times 1 + p(FA|\mathbf{d}) \times PI_{full/day} \times 1 \tag{16}$$

where $p(\text{Collapse}_k|\mathbf{d})$ denotes the probability of the kth building collapsing for the estimated characteristics of the incoming event, and $E(NC_{NA,\text{collapse},k}|\mathbf{d})$ is the expected number of associated collapse casualties calculated for the "no alert" case. $E(PI'_{loss,NA}|\mathbf{d}) = E[(PI_{full/day} - PI'_{red/day}) \times DT'_{NA}|\mathbf{d}]$ is a modified version of $E(PI_{loss,NA}|\mathbf{d})$ that accounts for reduced levels of damage to the electric cabins, $PI_{full/day}$ is the daily container-handling capacity of the port under ordinary operating conditions, and $PI'_{red/day}$ is the (EEW-mitigated) reduced container-handling capacity due to the incoming earthquake. $p(FA|\mathbf{d})$ is the probability of a false alarm, which is assumed to correspond to the case in which there is no performance loss for the "no alert" case, i.e., all components that contribute to the container handling operations are functional. Thus, a false alarm occurs in the jth simulation if the sampled ds of all electric cabins, cranes, wharves, and the control office are lower than moderate.

3.4. Step 4: Application of the decision-making algorithm

We implement an MCDM method to determine the optimal alternative between issuing or not an alarm for a given set of information about an incoming event at the port. This particular algorithm facilitates stakeholder priorities towards multiple dimensions of loss in the EEW decision-making process.

The MCDM method depends on a set of N_c pre-defined criteria set by the stakeholder, which are measured using quantitative metrics expressed in their most appropriate and representative units. The decision maker's relative priority towards each criterion is also accounted for, using a weighting scheme. In this case, we assume that the criteria of interest to the stakeholder relate to maximising port safety and functionality, and the corresponding metrics are equivalent to the loss types considered in the previous section (i.e., PI_{loss} and NC ; see Figure 5). We leverage the MCDM approach for EEW demonstrated in Cremen and Galasso [7], which involves constructing a decision matrix (see Table 1). Each ith row of the matrix corresponds to an available alternative (in this case, issuing or not issuing the alarm) and each ijth entry ($r_{A_i,c_j} w_j$) contains the weighted and normalised value of the jth corresponding loss metric, which is conditional on $\mathbf{d}$. The optimal decision is computed using the TOPSIS (Technique for Order Preference by Similarity to Ideal Solution) approach [42, 43], such that it maximises the S_i value according to:

$$S_i = \frac{y_i^-}{y_i^+ + y_i^-} \tag{17}$$

where $y_i^- = \sqrt{\sum_{j=1}^{N_c} (v_j^- - r_{A_i,c_j} w_j)^2}$ and $y_i^+ = \sqrt{\sum_{j=1}^{N_c} (v_j^+ - r_{A_i,c_j} w_j)^2}$. v_j^- and v_j^+ are respectively the maximum and minimum values of rAi,cjwj across all criteria.

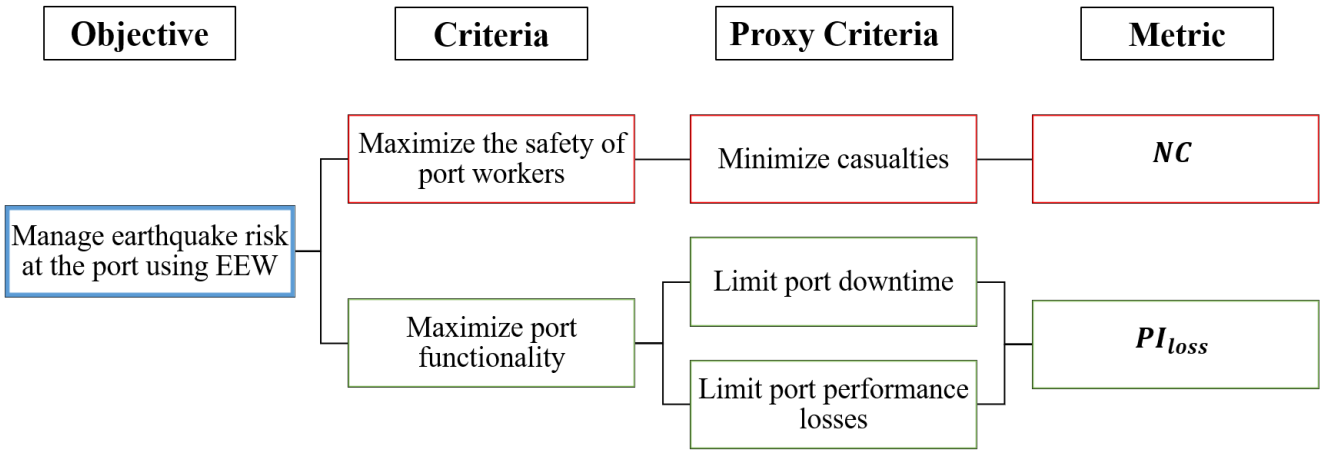

Figure 5: Graphical illustration of the MCDM inputs used for the case study.

Table 1: Representation of the decision matrix used as part of the MCDM approach applied to EEW at the port. Note that $w_{PI_{loss}}$ and w_{NC} respectively denote the stakeholder's relative priority (preference) for maximising port functionality and safety, and all other variables are as defined previously in the text.

Alternatives	Criteria	
	PI_{loss} (TEU)	NC (number)
Alert (A)	$\frac{E(PI_{loss,A}\|\mathbf{d})}{\sqrt{E(PI_{loss,A}\|\mathbf{d})^2+E(PI_{loss,NA}\|\mathbf{d})^2}} \times w_{PI_{loss}}$	$\frac{E(NC_A\|\mathbf{d})}{\sqrt{E(NC_A\|\mathbf{d})^2+E(NC_{NA}\|\mathbf{d})^2}} \times w_{NC}$
No alert (NA)	$\frac{E(PI_{loss,A}\|\mathbf{d})}{\sqrt{E(PI_{loss,NA}\|\mathbf{d})^2+E(PI_{loss,NA}\|\mathbf{d})^2}} \times w_{PI_{loss}}$	$\frac{E(NC_{NA}\|\mathbf{d})}{\sqrt{E(NC_A\|\mathbf{d})^2+E(NC_{NA}\|\mathbf{d})^2}} \times w_{NC}$

3.5. Step 5: Definition of optimal decision thresholds

3.5.1. Main results

We first determine the DSS alert thresholds for each of the three algorithms introduced in Section 3.2, assuming that the stakeholder of interest places equal weighting on the PI_{loss} and NC loss metrics (i.e., $w_{PI_{loss}} = w_{NC} = 0.5$). Figure 6 to 8 display the thresholds for Algorithm #1 (for rock conditions), Algorithm #2, and Algorithm #3, respectively, for an incoming event of 10 km depth and using 2000 Monte Carlo simulations for the risk assessment. Note that we assume equivalent ground-shaking amplitudes

(on rock) at each port component of interest. This means that the port is treated as a "point target site", which is reasonable given its < 5km length and represents a somewhat average trade-off between a conservative and an unconservative approach for any given event of arbitrary location, considering the im/pga values used in equations 4 to 7 for the port as a point target are unlikely to be either the maximum or the minimum ground-motion amplitudes experienced across the port.

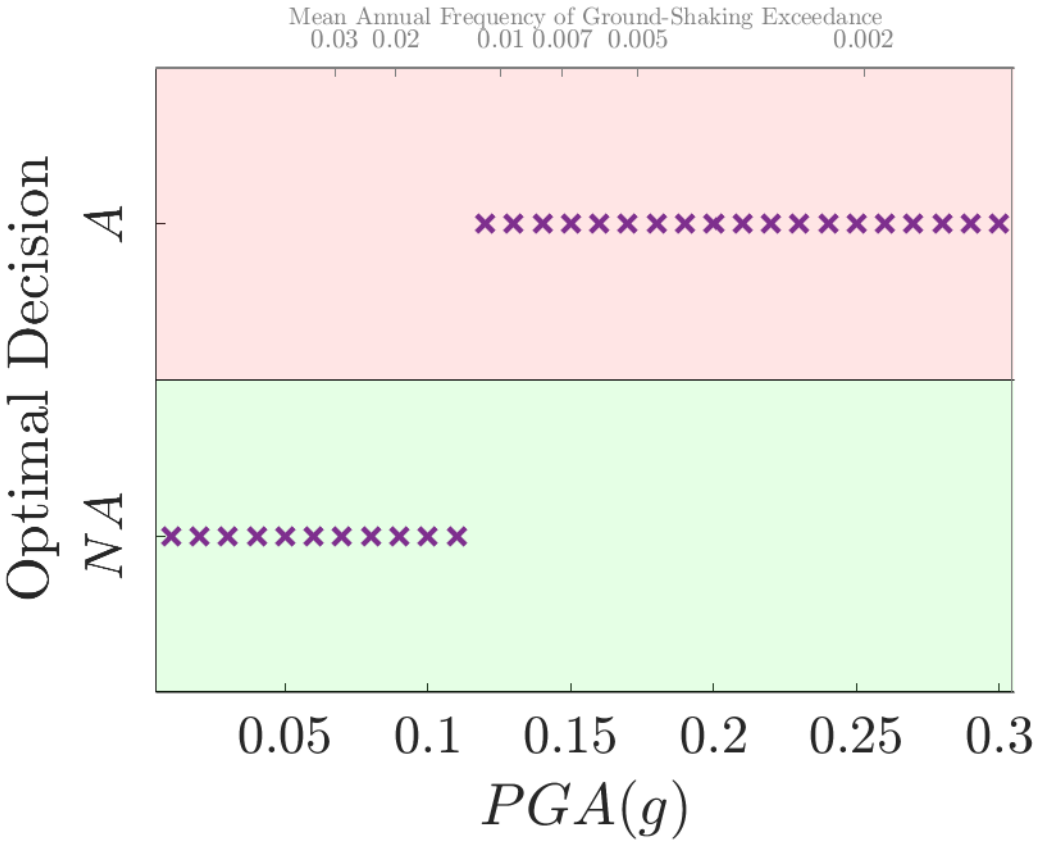

Figure 6: Identifying the optimal decision threshold (under rock conditions) for Algorithm #1. Note that A is the action of triggering an alarm and NA means that no alert is issued.

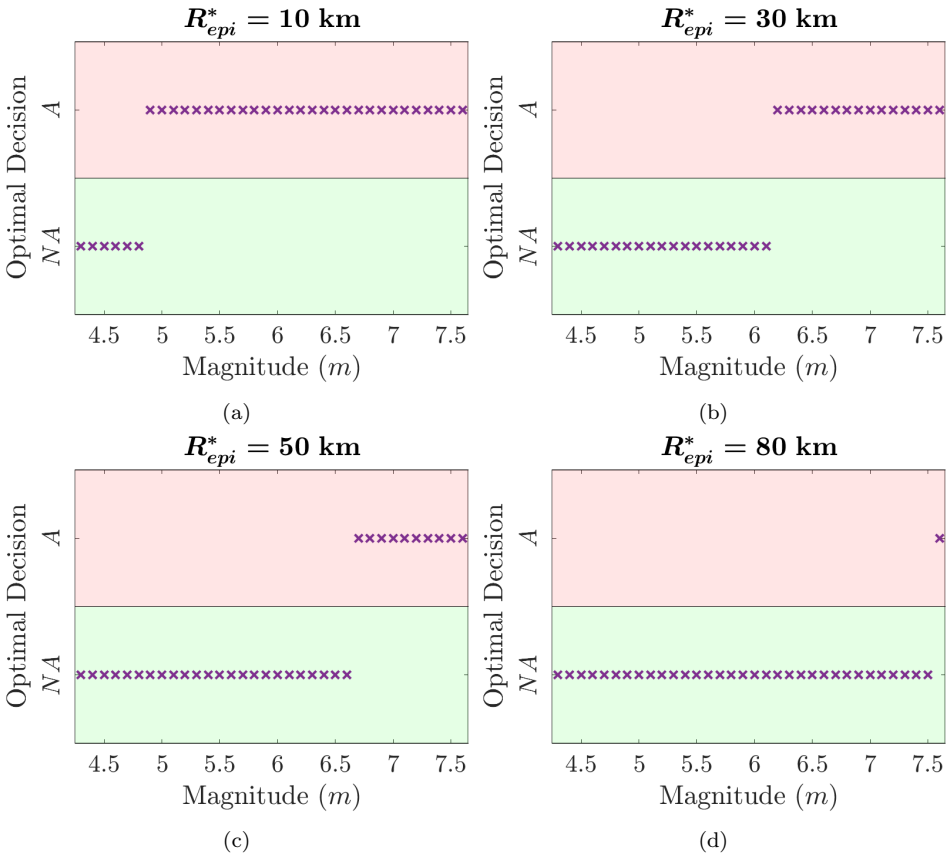

Figure 7: Identifying the optimal decision threshold for Algorithm #2, across four potential epicentral distances (R^*_{epi}) for an incoming event. Note that A is the action of triggering an alarm and NA means that no alert is issued.

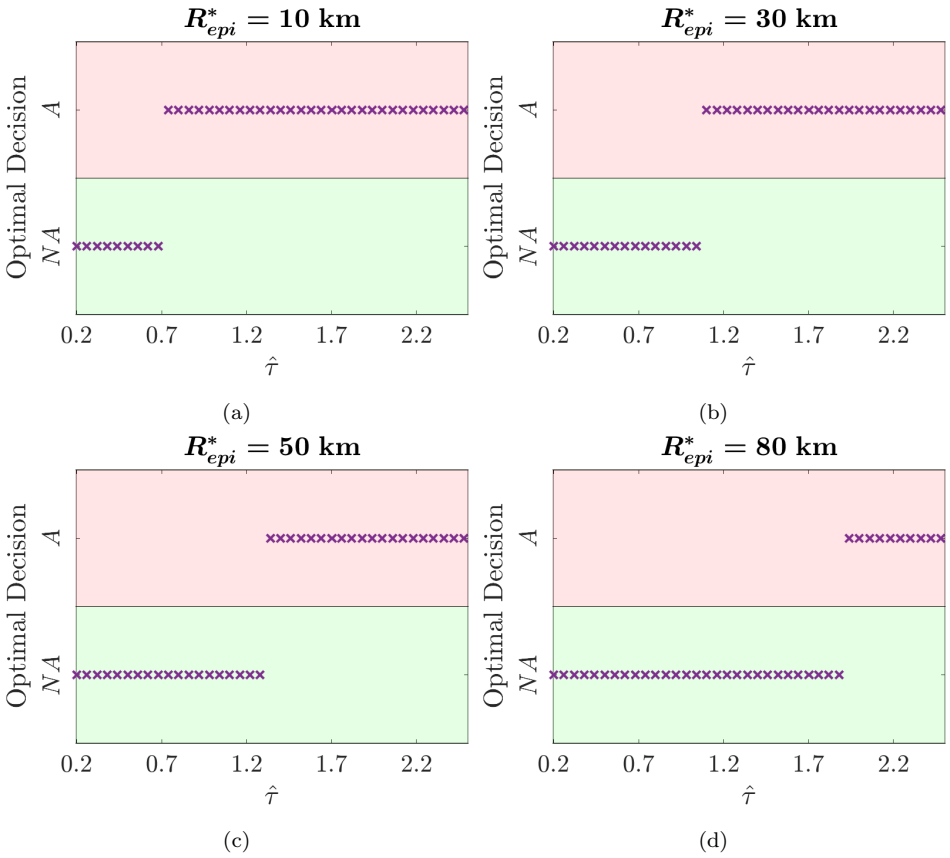

Figure 8: Identifying the optimal decision threshold for Algorithm #3, across four potential epicentral distances (R^*_{epi}) for an incoming event. Note that A is the action of triggering an alarm and NA means that no alert is issued.

It can be seen from Figure 6 that the alarm is issued for estimated rock PGA values larger than approximately 0.12 g. We leverage this value to determine how often the alert might be triggered, using the median site-specific hazard curve (38.408° latitude, 15.910 longitude°) for rock conditions computed from the INGV seismic hazard model (retrieved at: `http://esse1-gis.mi.ingv.it/mps04_eng.jsp`). It may be inferred from Figure 6 that an alarm is expected to be issued approximately once every 100 years.

Figure 7 demonstrates that the magnitude at which an alert is triggered increases with epicentral distance (R^*_{epi}), which is explained by the expected distance-decaying amplitude of ground-shaking intensities (for a given event). It may be observed that an alarm should be issued for magnitudes near 5

when $R^*_{epi} = 10$ km, it should be triggered for magnitudes around 6 when $R^*_{epi} = 30$ km, it should be triggered for magnitudes close to 6.5 when $R^*_{epi} = 50$ km, and it should only be triggered for the maximum magnitude (i.e., 7.6) when $R^*_{epi} = 80$ km.

The results of Figure 8 assume that $n = 30$ in Equation 1 (i.e., that an EEW system implemented for the port would at least consist of 30 stations located within the immediate epicentral area). Under this condition, it is found that the alarm should be triggered for $\hat{\tau} \gtrapprox 0.7$ when $R^*_{epi} = 10$ km, whereas it should only be triggered for $\hat{\tau} \gtrapprox 1.8$ when $R^*_{epi} = 80$ km. These findings are reasonable, given that $\hat{\tau}$ is positively correlated with magnitude (which can be inferred from Equation 2). In a practical application of the DSS, the threshold values of $\hat{\tau}$ could be computed offline ahead of EEW deployment, across a series of possible epicentral distances and n values, to significantly expedite the real-time decision-making process.

3.5.2. Sensitivity analyses

We investigate variations in DSS alert thresholds relative to the case presented in Section 3.5.1 (henceforth referred to as "Case 1"), for the following individual modifications to the calculations: (1) $w_{PI_{loss}} = 0.05$ and $w_{NC} = 0.95$ ("Case 2"); (2) $w_{PI_{loss}} = 0.95$ and $w_{NC} = 0.05$ ("Case 3"); (4) PI_{loss} is not dependent on the functionality of the control office ("Case 4"); and (5) PI_{loss} is only dependent on the functionality of the cranes' structural components ("Case 5"). Results for the five cases are compared in Figure 9 (for Algorithm #1) and Figure 10 (for Algorithm #2). It can be seen from these figures that the most conservative and most unconservative thresholds are produced for Case 3 and Case 5, respectively (note that the same trends in findings across the various cases are observed for Algorithm #3).

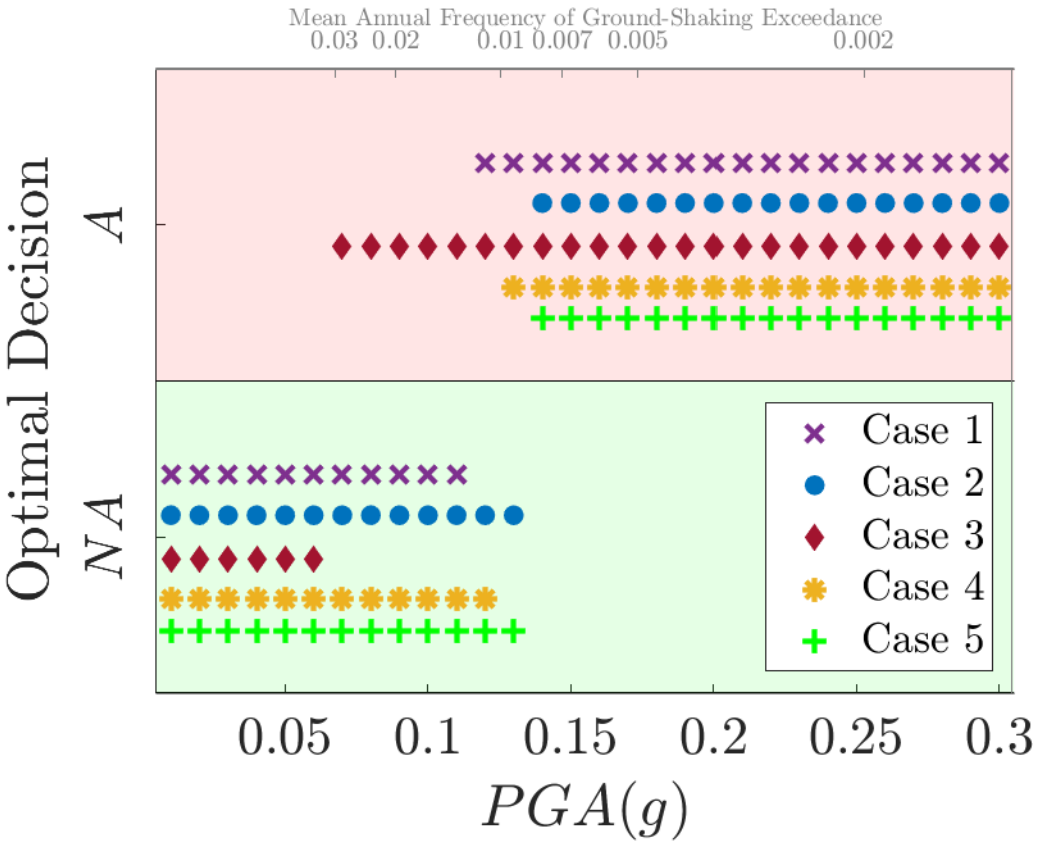

Figure 9: Sensitivity analyses of the optimal decision threshold (under rock conditions) for Algorithm #1. All cases are explained in the text. Note that A is the action of triggering an alarm and NA means that no alert is issued.

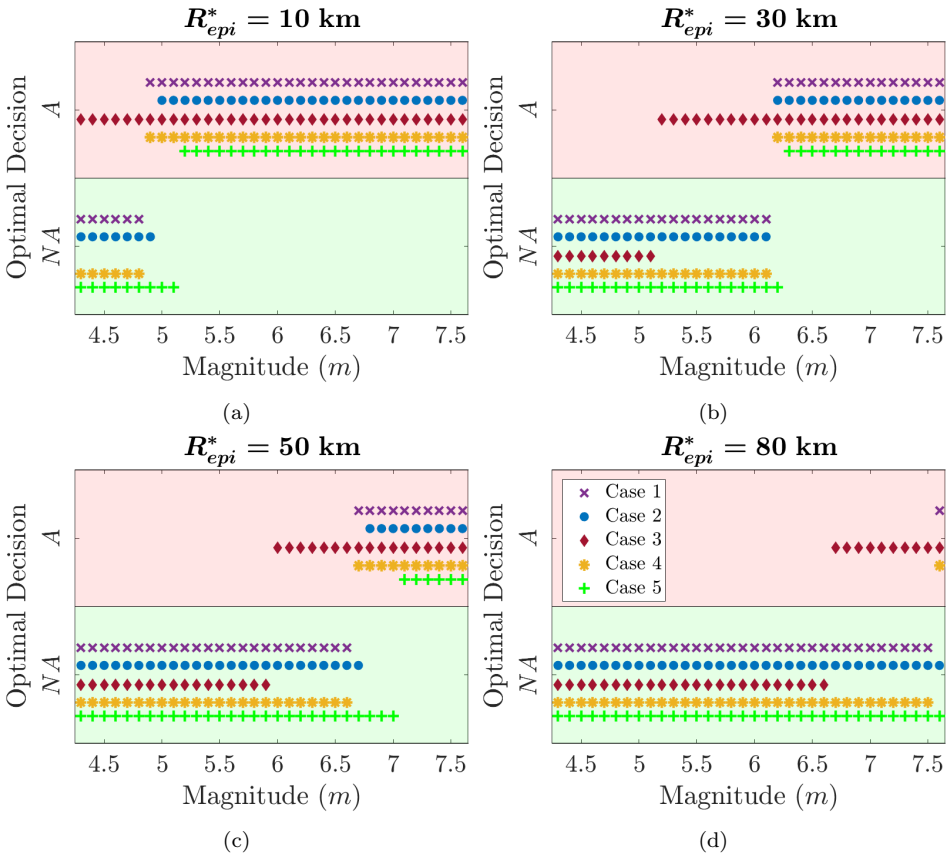

Figure 10: Sensitivity analyses of the optimal decision threshold for Algorithm #2, across four potential epicentral distances (R^*_{epi}) for an incoming event. All cases are explained in the text. Note that A is the action of triggering an alarm and NA means that no alert is issued.

The results of Case 2 and Case 3 indicate that alert triggering is driven by the PI_{loss} metric, which is partly explained by the assumption of some casualties occurring when an alarm is issued and the fact that the probability of a false alarm (which influences the $E[PI_{loss,A}|\mathbf{d}]$ value) reduces to 0 for PGA values greater than 0.04 g. It is interesting to note that Case 3 would cause an alarm to trigger approximately three to four times as frequently as Case 2 and produces a magnitude-based alert threshold that is about one unit larger than that of Case 2 (across all considered epicentral distances), underlining the importance of accounting for stakeholder preferences in the EEW decision-making process.

The findings of Case 4 and Case 5 reveal that neglecting the complete set of functional interdependencies among port components creates an opportunity for missed alarms, i.e., the alert-triggering threshold can be set too high. For example, the results imply that an alarm would be issued approximately 50% less often than required if only the structural components of a crane were considered for computing its functionality (i.e., Case 5) and the alert threshold would be slightly overestimated (by 0.01 g) if the operational status of the control office was neglected (i.e., Case 4).

4. Conclusions

This study has proposed a novel risk-informed EEW DSS, for specific application to a seaport system. The purpose of the DSS is to determine optimal conditions under which to trigger an EEW alert for an incoming seismic event, considering tangible engineering-oriented consequences that the earthquake might have for the port as well as those related to the action of issuing an alarm. Developing the DSS involves a number of logical steps, which uniquely unify (1) PBEEW, (2) a simulation-based risk approach that captures the interconnectedness of the port system, and (3) a decision-making algorithm that facilitates diverse stakeholder perspectives on different types of risk.

The DSS was demonstrated by determining optimal EEW alert-triggering thresholds for the port of Gioia Tauro in Southern Italy, one of the most important transhipment hubs in the Mediterranean Sea. This application specifically considered the consequences of port performance loss and casualties, using a number of EEW seismological algorithms to demonstrate decision making on the basis of (1) ground-shaking estimates; (2) approximate magnitude-distance pairs; and (3) raw early seismic signal data that often acts as input to operational EEW systems. It was found, as expected, that the optimal alert-triggering threshold in terms of magnitude increases with epicentral distance. We also determined that an alert would be triggered approximately once every 100 years if both consequences were considered to be equally important to a stakeholder, but this frequency would increase to once every 50 years if performance losses were prioritised, or reduce to approximately once every 125 years if casualties were assigned a higher weighting. These findings emphasise the importance of considering stakeholder (end-user) risk preferences when calibrating alert thresholds in an EEW system, and are consistent with the conclusions of Cremen and Galasso [7], which was

the first study to comprehensively demonstrate the integration of an MCDM method in an EEW process.

Ports are complex systems that incorporate a number of structural/infrastructural components with integral functional interdependencies. Our application of the DSS also explored the importance of these interdependencies in EEW decision making, by investigating variations in optimal alert thresholds that arise if some of the port-system interconnectedness is neglected. In particular, we found that ignoring the operational dependence of cranes on functioning power supplies, wharves, and the port's control office can lead to significantly unconservative results, such that alerts would only be issued half as often as required. This finding is consistent with those of Conca et al [21], who demonstrated that neglecting interdependencies among port components in a seismic risk assessment led to lower predictions of port capacity losses. In this study, we infer that accounting for the interdependent characteristics of a port system would be crucial for successful calibration of its EEW system. It is interesting to note, however, that the sensitivity of the trigger threshold to functional interdependency assumptions was found to be less than that due to diverse stakeholder risk priorities. We can therefore conclude (at least for the case study examined and the particular set of sensitivity analyses conducted in this paper) that, for correct decision-making with the proposed EEW DSS, it is more important to gather appropriate information on stakeholder preferences than accurately characterise the complete set of functional interrelationships within the port system.

It is important to emphasise that the case-study application illustrated in this work is for demonstrative purposes only, and is associated with some limitations and assumptions. For example, available lead times were not considered in the decision-making process; in realistic scenarios, limited lead times may constrain the type of actions that can be taken for an EEW alert and may invalidate some of the preventative measures considered in this study. Secondly, the fragility functions, restoration times, casualty module, and seismological models (e.g., GMM) employed were not explicitly developed for the target area of interest, which may affect the accuracy of the loss calculations carried out. A more refined analysis may leverage more region-appropriate port-related fragility functions [e.g., 16]. Soil liquefaction, which is a common occurrence in port areas after earthquakes [e.g., 44], is outside the scope of this study (although its effects are not anticipated to have a significant influence on the results [24]). We also neglect detailed ground responses that can spatially vary across the port (see Conca et al. [21]). Nevertheless, this paper

provides useful insights on how a comprehensive evaluation of seismic risk (adapted to capture real-time event-parameter uncertainties) coupled with a formal decision-making algorithm can be effectively leveraged to determine EEW alarm thresholds for the case of a large seaport. The next step will be to integrate and test the developed DSS within the TURNkey earthquake early warning platform deployed at the Port of Gioia Tauro, to confirm its applicability to real-world scenarios.

References

[1] R. M. Allen, D. Melgar, Earthquake early warning: Advances, scientific challenges, and societal needs, Annual Review of Earth and Planetary Sciences 47 (2019). doi:10.1146/annurev-earth-053018.
URL https://doi.org/10.1146/annurev-earth-053018-

[2] K. A. Porter, Best Practices for Earthquake Early Warning: A Compendium, Tech. rep. (2020).
URL www.sparisk.com

[3] G. Cremen, C. Galasso, Earthquake early warning: Recent advances and perspectives, Earth-Science Reviews (2020) 103184.

[4] C. S. Oliveira, F. Mota de Sá, M. Lopes, M. A. Ferreira, I. Pais, Early warning systems: Feasibility and end-users' point of view, Pure and Applied Geophysics 172 (9) (2015) 2353–2370. doi:10.1007/s00024-014-0999-0.

[5] A. Saini, I. Tien, Methodology for real-time prediction of structural seismic risk based on sensor measurements, Structural safety 73 (2018) 54–63.

[6] G. Cremen, O. Velazquez, B. Orihuela Gonzalez, C. Galasso, Predicting approximate seismic responses in multistory buildings from real-time earthquake source information, for earthquake early warning applications, Bulletin of Earthquake Engineering in press (2021).

[7] G. Cremen, C. Galasso, A decision-making methodology for risk-informed earthquake early warning, Computer-Aided Civil and Infrastructure Engineering 36 (6) (2021) 747–761.

[8] S. A. Zarghami, J. Dumrak, Unearthing vulnerability of supply provision in logistics networks to the black swan events: Applications of entropy theory and network analysis, Reliability Engineering & System Safety (2021) 107798.

[9] X. Jia, D. Zhang, Prediction of maritime logistics service risks applying soft set based association rule: An early warning model, Reliability Engineering & System Safety 207 (2021) 107339.

[10] X. Cao, J. S. L. Lam, Simulation-based catastrophe-induced port loss estimation, Reliability Engineering & System Safety 175 (2018) 1–12.

[11] K. Pitilakis, S. Argyroudis, S. Fotopoulou, S. Karafagka, K. Kakderi, J. Selva, Application of stress test concepts for port infrastructures against natural hazards. the case of thessaloniki port in greece, Reliability Engineering & System Safety 184 (2019) 240–257.

[12] N. U. I. Hossain, F. Nur, S. Hosseini, R. Jaradat, M. Marufuzzaman, S. M. Puryear, A bayesian network based approach for modeling and assessing resilience: A case study of a full service deep water port, Reliability Engineering & System Safety 189 (2019) 378–396.

[13] N. U. I. Hossain, S. El Amrani, R. Jaradat, M. Marufuzzaman, R. Buchanan, C. Rinaudo, M. Hamilton, Modeling and assessing interdependencies between critical infrastructures using bayesian network: A case study of inland waterway port and surrounding supply chain network, Reliability Engineering & System Safety 198 (2020) 106898.

[14] C. Poulin, M. Kane, Infrastructure resilience curves: Performance measures and summary metrics, Reliability Engineering & System Safety (2021) 107926.

[15] C. Meletti, F. Galadini, G. Valensise, M. Stucchi, R. Basili, S. Barba, G. Vannucci, E. Boschi, A seismic source zone model for the seismic hazard assessment of the italian territory, Tectonophysics 450 (1-4) (2008) 85–108.

[16] F. Bozzoni, C. G. Lai, P. Marsan, D. Conca, A. Fama, WebGIS platform for seismic risk assessment of maritime port systems in Italy, in: Proc., 4th PIANC Mediterranean Days Congress, 2018.

[17] A. Shafieezadeh, L. I. Burden, Scenario-based resilience assessment framework for critical infrastructure systems: Case study for seismic resilience of seaports, Reliability Engineering & System Safety 132 (2014) 207–219.

[18] I. Iervolino, V. Convertito, G. Massimiliano, G. Manfredi, A. Zollo, Real-time risk analysis for hybrid earthquake early warning systems, Journal of Earthquake Engineering 10 (6) (2006) 867–885.
URL www.worldscientific.com

[19] I. Iervolino, M. Giorgio, G. Manfredi, Expected loss-based alarm threshold set for earthquake early warning systems, Earthquake Engineering and Structural Dynamics 36 (9) (2007) 1151–1168. doi:10.1002/eqe.675.

[20] I. Iervolino, Performance-based earthquake early warning, Soil Dynamics and Earthquake Engineering 31 (2) (2011) 209–222. doi:10.1016/j.soildyn.2010.07.010.

[21] D. Conca, F. Bozzoni, C. G. Lai, Interdependencies in seismic risk assessment of seaport systems: Case study at largest commercial port in Italy, ASCE-ASME Journal of Risk and Uncertainty in Engineering Systems, Part A: Civil Engineering 6 (2) (2020) 04020006.

[22] E. Triantaphyllou, Multi-criteria decision making methods, in: Multi-criteria decision making methods: A comparative study, Springer, 2000, pp. 5–21.

[23] R. Basili, P. Burrato, U. Fracassi, V. Kastelic, F. Maesano, G. Tarabusi, M. M. Tiberti, G. Valensise, R. Vallone, P. Vannoli, et al., Database of Individual Seismogenic Sources (DISS), Version 3.2. 1: A compilation of potential sources for earthquakes larger than M 5.5 in Italy and surrounding areas (2018).

[24] F. Bozzoni, A. Famà, C. Lai, S. Mirfattah, Seismic risk assessment of seaports using GIS: the port of Gioia Tauro in Southern Italy, in: 33th PIANC World Congress San Francisco, USA, 2014, pp. 1–5.

[25] I. Iervolino, M. Giorgio, C. Galasso, G. Manfredi, Uncertainty in early warning predictions of engineering ground motion parameters: What

really matters?, Geophysical Research Letters 36 (4) (2009) L00B06. doi:10.1029/2008GL036644.
URL http://doi.wiley.com/10.1029/2008GL036644

[26] K. Porter, J. Jones, S. Detweiler, A. Wein, How many injuries can be avoided in the haywired scenario through earthquake early warning and drop, cover, and hold on?, The HayWired earthquake scenario—Earthquake implications: US Geological Survey Scientific Investigations Report (2018).

[27] K. A. Porter, How Many Injuries can be Avoided through Earthquake Early Warning and Drop, Cover, and Hold On?, Tech. rep., Structural Engineering and Structural Mechanics Program, Department of Civil Environmental and Architectural Engineering,University of Colorado, Boulder, Boulder, Colorado (2016).

[28] D. Riopelle, Likelihood of organizations in the los angeles area implementing an earthquake early warning system, Ph.D. thesis, UCLA (2020).

[29] G. Cremen, C. Galasso, E. Zuccolo, Investigating the potential effectiveness of earthquake early warning across Europe, Nature Communications in review (2021).

[30] R. M. Allen, H. Kanamori, The potential for earthquake early warning in southern California, Science 300 (5620) (2003) 786–789.

[31] S. Barani, D. Spallarossa, P. Bazzurro, Disaggregation of probabilistic ground-motion hazard in italy, Bulletin of the Seismological Society of America 99 (5) (2009) 2638–2661.

[32] M. Picozzi, A. Zollo, P. Brondi, S. Colombelli, L. Elia, C. Martino, Exploring the feasibility of a nationwide earthquake early warning system in Italy, Journal of Geophysical Research: Solid Earth 120 (4) (2015) 2446–2465. doi:10.1002/2014JB011669.

[33] FEMA, HAZUS: Earthquake loss estimation methodology, Federal Emergency Management Agency (FEMA) Washington, DC, 2004.

[34] F. Bozzoni, C. G. Lai, Tools for rapid seismic response assessment of strategic facilities under GIS environment: applications to Italian

seaports and embankment dams, in: 3rd International conference on performance-based design in earthquake geotechnical engineering, 2017.

[35] B. Borzi, R. Pinho, H. Crowley, Simplified pushover-based vulnerability analysis for large-scale assessment of RC buildings, Engineering Structures 30 (3) (2008) 804–820.

[36] B. Borzi, M. Faravelli, A. Di Meo, Application of the sp-bela methodology to rc residential buildings in italy to produce seismic risk maps for the national risk assessment, Bulletin of Earthquake Engineering (2020) 1–24.

[37] S. Akkar, M. A. Sandıkkaya, J. J. Bommer, Empirical ground-motion models for point-and extended-source crustal earthquake scenarios in Europe and the Middle East, Bulletin of earthquake engineering 12 (1) (2014) 359–387.

[38] S. E. Minson, J. R. Murray, J. O. Langbein, J. S. Gomberg, Real-time inversions for finite fault slip models and rupture geometry based on high-rate GPS data, Journal of Geophysical Research: Solid Earth 119 (4) (2014) 3201–3231. doi:10.1002/2013JB010622.

[39] MTC, Norme Tecniche per le Costruzioni, D.M. 17-01-2018 (Italian building code), Tech. rep. (2018).

[40] FEMA, HAZUS 4.2: Earthquake model technical manual, Federal Emergency Management Agency (FEMA) Washington, DC, 2018.

[41] Centre for Industrial Studies and DKM Economic Consultants, Ex-Post Evaluation of Investment Projects Co-Financed by the European Regional Development Fund (ERDF) and Cohesion Fund (CF) in the Period 1994-1999: Inception Report, Tech. rep., Centre for Industrial Studies; DKM Economic Consultants (2011).

[42] K. P. Yoon, C.-L. Hwang, Multiple attribute decision making: an introduction, Sage Publications, 1995.

[43] N. Caterino, I. Iervolino, G. Manfredi, E. Cosenza, Multi-criteria decision making for seismic retrofitting of RC structures, Journal of Earthquake Engineering 12 (4) (2008) 555–583. doi:10.1080/13632460701572872.

[44] C.-K. Chung, H.-S. Kim, C.-G. Sun, Real-time assessment framework of spatial liquefaction hazard in port areas considering site-specific seismic response, Computers and Geotechnics 61 (2014) 241–253.